PAPER

Re-examining the giant magnetization density in α″-Fe$_{16}$N$_2$ with the SCAN+U method

Assa Aravindh Sasikala Devi, [iD] *[a] Johannes Nokelainen,[bc] Bernardo Barbiellini,[bc] Murali Devaraj,[d] Matti Alatalo[a] and Arun Bansil[c]

We present an in-depth discussion of the magnetic ground state of α″-Fe$_{16}$N$_2$ within the framework of the density functional theory (DFT). The exchange–correlation effects are treated using a variety of schemes, including the local-spin-density approximation, the generalized-gradient approximation, and the Strongly-Constrained-and-Appropriately-Normed (SCAN) scheme. We also delineate effects of adding an on-site interaction parameter U on the Fe sites. Among all the schemes considered, only SCAN+U is found to capture the surprisingly large magnetization density in α″-Fe$_{16}$N$_2$ that has been observed experimentally. Our study shows how the combination of SCAN and self-interaction corrections applied on different Fe sites through the parameter U can reproduce both the correct equilibrium volume and the giant magnetization density of α″-Fe$_{16}$N$_2$.

I. Introduction

Permanent magnets for functional applications are currently based largely on the costly rare earths such as Sm, Nd, and Gd and there is great need to find new cost-effective alternatives.[1–3] In this connection, magnetic nitrides, such as the iron nitrides, appear to be promising,[4] and among these α″-Fe$_{16}$N$_2$,[5,6] discovered in 1951,[7] stands out because it supports a giant magnetization density.[8–10] Kim and Takayashi[8] have reported a magnetization of 2.58 T and Sugita *et al.* reported an even higher magnetization of 2.8–3.0 T.[11] These large values of the magnetization are surprising because they exceed the maximum magnetization expected from the Slater–Pauling curve,[12] which attributes the magnetic saturation of an itinerant ferromagnet solely to the number of empty states in the 3d shell and this number is maximized for the FeCo alloys at a magnetization density of about 2.45 T. Giant magnetization in α″-Fe$_{16}$N$_2$ thus implies the emergence of localized magnetic moments in the material. It has been suggested that the giant magnetization of α″-Fe$_{16}$N$_2$[13–15] is not an intrinsic property but that it reflects difficulties of preparing single crystals of Fe$_{16}$N$_2$ and in performing accurate measurements in multi-phase samples. This topic has been quite controversial: two symposia were held in this connection at the MMM conferences in 1994 and 1996.[16]

Although Sugita and Jiangs groups reported experiments showing high magnetization, these results were not corroborated by any other group,[8,15] and the topic did not draw much attention after 2000. The work of Wang *et al.*,[10] however, which uses many different characterization techniques, including the XMCD, appears to address the issue of giant magnetization. Successful attempts to prepare α″-Fe$_{16}$N$_2$ samples have been reviewed by Wang[16] and include the synthesis of thick α″-Fe$_{16}$N$_2$ foils.[17] The most recent X-ray and neutron diffraction results by Hang *et al.* report saturation magnetizations of 2.6–2.9 T,[18] and have been reproduced by a cluster-atom model introduced by Ji *et al.*[19]

Recent Density Functional Theory (DFT) studies of α″-Fe$_{16}$N$_2$ based on the Generalized Gradient Approximation (GGA) corrected by the Hubbard parameter U have been reported by Bhattacharjee *et al.*,[20] Islam *et al.*,[21] and Stoeckl *et al.*[22] These investigations and other DFT+U calculations[19,23–27] show, as expected, that the Fe magnetic moment increases with the strength of correlation effects described by U. However, increasing U expands the equilibrium volume when the geometry is optimized,[22] so that the magnetization density M_s does not increase beyond the Slater–Pauling limit of 2.45 T.

Here, we show that a DFT+U scheme based on the Strongly-Constrained-and-Appropriately-Normed (SCAN) method[28] can avoid the spurious volume expansion encountered in GGA+U, which is also the case for the LSDA+U results of Ji *et al.*[19] SCAN has the satisfactory feature that it satisfies all the 17 exact constraints appropriate to a semilocal functional,[28] which is not the case for the GGA.[29] For these reasons,[30] SCAN has been shown to be systematically superior to GGA and it can be even better than the hybrid functionals,[31–33] which present difficulties, for example, in bulk metals[34] and cuprate superconductors.[35]

[a] *Nano and Molecular Systems Research Unit, University of Oulu, P.O. Box 8000, FI-90014, Finland. E-mail: Assa.Sasikaladevi@oulu.fi*
[b] *Lappeenranta-Lahti University of Technology (LUT), FI-53851 Lappeenranta, Finland*
[c] *Department of Physics, Northeastern University, Boston, MA 02115, USA*
[d] *Department of Sciences, Indian Institute of Information Technology Design and Manufacturing, Kurnool, Andhra Pradesh, 518002, India*

This journal is © the Owner Societies 2022

Phys. Chem. Chem. Phys., 2022, **24**, 17879–17884 | **17879**

SCAN+U,[36] however, correctly captures the giant magnetization density of α''-Fe$_{16}$N$_2$ beyond the Slater–Pauling limit, despite its somewhat larger computational cost compared to GGA+U.

II. Computational details

Spin-polarized electronic structure calculations were performed within the framework of the DFT using the projected augmented wave (PAW) method implemented in the Vienna Ab initio Simulation Package (VASP).[37,38] The GGA-PBE (Perdew–Burke–Ernzerhof) method[29] was used to account for exchange–correlation effects. The effects of gradient corrections to the local-spin-density approximation (LSDA), which are included in the GGA are important for correctly capturing the magnetic phases of pristine Fe.[39]

Strong Coulomb correlation effects are described within the DFT+U scheme as implemented by Dudarev et al.[40] The DFT+U scheme is a simplified version of the self-interaction correction,[41] where the correction U acts only on the localized 3d states, and often results in splitting the metallic energy bands into upper and lower Hubbard bands descriptive of Mott–Hubbard physics.[42–44] We also use the SCAN meta-GGA scheme,[28] which has been shown to provide an improved description of correlated materials such as α-Mn,[45] cuprates,[46–49] nickelates[50] spinel LiMn$_2$O$_4$ cathode material,[51] iridates,[52] and 3d perovskite oxides.[53]

Within the PAW pseudopotential scheme, we describe Fe and N with 8 and 5 valence electrons, respectively. A plane wave cut-off energy of 600 eV is used.

k-Points within the Brillouin zone were generated using a uniform 8 × 8 × 8 Monkhorst–Pack[54] mesh. Electronic energy minimization was performed with a tolerance of 10^{-6} eV. The conjugate-gradient algorithm was used to relax atomic structures until all residual forces converged to within 0.005 eV Å^{-1}. A Gaussian smearing width of 0.05 eV (FWHM) was applied to the electronic states. In order to obtain more accurate total energies and density of states (DOS), the tetrahedron method with Blöchl corrections[55] was used. Collinear spins were used in most calculations but in order to compute the magneto-crystalline anisotropy (MCA), non-collinear calculations were also performed.

III. Results and discussion

Gradient corrections to the LSDA are needed to stabilize the ferromagnetic phase of α-Fe, which has partially filled 3d majority states with a magnetic moment of $m = 2.3\mu_B$ in the self-consistent linearized muffin-tin-orbital (LMTO) calculations.[39] Surprisingly, SCAN corrections beyond the GGA can substantially overestimate the magnetic moment of α-Fe as shown by several authors.[56–59] Recently, this problem has been cured by introducing a de-orbitalized SCAN potential.[60] The de-orbitalization condition is especially important at the Fermi Surface of itinerant ferromagnetic materials as shown by eqn (24) in the paper by Gunnarsson and Lundqvist.[61] This constraint has been discussed also by Barbiellini and Bansil.[43] However, the SCAN overestimation of
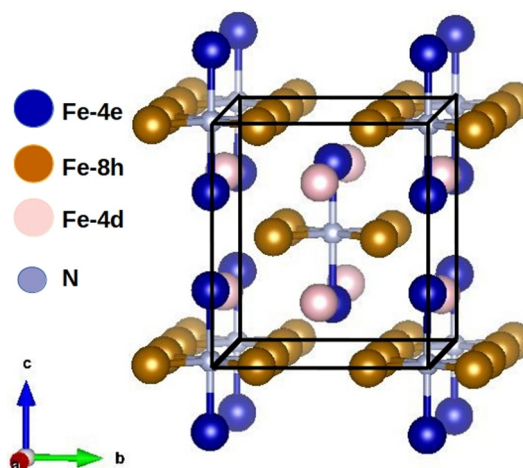

Fig. 1 Equilibrium structure of Fe$_{16}$N$_2$. Fe atoms occupy three inequivalent Wyckoff sites labeled 8h (golden),4e (blue) and 4d (pink).

the magnetic moment encountered in itinerant ferromagnetic systems does not apply in the present case since the 3d electrons are clearly more localized due to the magnetization density being above the Slater–Pauling limit.

Bulk Fe in the α phase assumes BCC structure with the easy-magnetization axis oriented along the (001) axis.[62] Insertion of N expands the volume and brings the easy magnetization axis parallel to the c-axis, producing the MCA. Bonding with N also increases the Fe magnetic moments to the order of $3\mu_B$, which points to the need for invoking substantial corrections beyond the GGA. The experimental α''-Fe$_{16}$N$_2$ crystal structure[7,63] is body-centered tetragonal (space group $I4/mmm$) with lattice parameters of $a = b = 5.72$ Å and $c = 6.29$ Å. The experimental structure shown in Fig. 1 can be seen as a distorted version of a 2 × 2 × 2 supercell of BCC Fe with two N atoms occupying the octahedral interstitial positions. The Fe atoms can be divided into three inequivalent Wyckoff sites 8h, 4e and 4d by their coordination with respect to the N atoms. The Fe-8h and 4e atoms form an octahedron around the N atoms (Fig. 1), where the Fe-8h atoms occupy the equatorial sites and the Fe-4e atoms occupy the axial sites. The Fe-4d atoms are not coordinated with the N atoms. This cell size is sufficient for describing the ferromagnetic phase α''-Fe$_{16}$N$_2$. However, larger supercells are needed for more complex orders, as is the case for magnetic phases of the cuprates, etc.[48]

We first carried out calculations using the fixed experimental volume to ascertain if the giant magnetization might be possible to capture in this way. The results for the LSDA, GGA, GGA+U, SCAN, and SCAN+U corrections are summarized in Table 1. The used U values have been computed by Lai et al.[26] using formulae based on screened Coulomb integrals involving the densities of the Fe 3d electrons and have the following values at different atomic sites: Fe-8h: 1.36 eV, Fe-4e: 1.088 eV, and Fe-4d: 3.94 eV. Interestingly, the values of M_s do not exceed the Slater–Pauling limit[12] of 2.45 T, even for GGA+U or SCAN, which are expected to improve the description of localized d-states substantially with respect to LSDA and GGA. Only the

Table 1 Magnetic moment and magnetization density (M_s) for different exchange–correlation approximations at the fixed experimental volume of 205.80 Å^3. In the DFT+U calculations, the U values on various Fe sites are: 1.36 eV (8h), 1.088 eV (4e) and 3.94 eV (4d)

Method	Total moment (μ_B)	M_s (T)
LSDA	36.49	2.21
GGA	39.05	2.21
GGA+U	42.75	2.42
SCAN	42.66	2.41
SCAN+U	45.82	2.59

SCAN+U is found to correctly predict M_s values above the Slater–Pauling limit, thus capturing the subtle balance between tendencies of electrons to form itinerant or localized states in the material.[10]

Next, we fully relaxed all structures in order to understand the connection between the equilibrium volume and magnetic properties. The LSDA produced a total magnetization of $36.49\mu_B$ per unit cell, which corresponds to an average magnetic moment of $2.28\mu_B$ per Fe atom. This value is significantly lower than the LSDA-based Fe magnetic moment in BCC Fe, indicating that LSDA encounters problems here in contrast to the case of pristine Fe.[39] The equilibrium volume obtained by LSDA (179.24 Å^3) is substantially smaller than the experimental value of 205.24 Å^3. In view of these shortcomings of the LSDA, we only report the results of our calculations based on the LSDA+U in Table 2.[19] The gradient corrections in the GGA improve the volume, but both the volume and the magnetization still remain small compared to the experimental value.[18] SCAN yields an increase in the magnetization M_s above the GGA value, but the equilibrium volume slightly shrinks with respect to the GGA. The GGA+U gives volume in excellent agreement with experiment, but it does not improve the magnetization density significantly. Finally, SCAN+U yields reasonable agreement with the experiment both for the volume, magnetization density and the c/a = 1.08 ratio, which is close to the corresponding experimental value of 1.10. The LSDA SCAN+U results

in Table 2 thus explain the anomalously large magnetization density. Our calculations in accordance with the LSDA+U method of ref. 19 (see Table 2) are also found to correctly predict the equilibrium volume and the M_s value above the Slater–Pauling limit, but the c/a ratio from LSDA+U is very far from the experimental value. Interestingly, the Heyd, Scuseria and Ernzerhof (HSE) hybrid-functional method[31–33] gives a M_s value above the Slater–Pauling limit, but the equilibrium volume is smaller than the experimental value.

The computed highest Fe magnetic moment is located on Fe-4d, while the neutron diffraction experiments[18] find that Fe-8h carries the largest magnetization. We now discuss if another SCAN+U correction could possibly improve the description of the magnetic moment distribution on the Fe atoms. Motivated by the agreement between the model of Ji $et~al.$[19] and the results of neutron diffraction experiments,[18] we have carried out a parametric SCAN+U(Fe-8h) study in which the Hubbard U is only applied to the Fe-8h position. The results are given in Table 3 and show a stronger magnetic moment at the Fe-8h position in better agreement with experiments.[18] The Fe-8h magnetic moment increases monotonically from $2.67\mu_B$ to $3.24\mu_B$ with increasing U values. The average magnetic moment reaches $2.93\mu_B$ for U(Fe-8h) value of 4 eV. The Fe-4d site, which is situated outside of the octahedral cluster, preserves magnetic moment of about $2.8\mu_B$ irrespective of the change in the U(Fe-8h) value. Interestingly, the Fe-4e magnetic moment is the lowest and reaches a minimum of about $2.8\mu_B$ around U(Fe-8h) = 2 eV. The equilibrium volume and the magnetization density as a function of the Hubbard parameter applied to the Fe-8h sites are presented in Fig. 2. The experimental volume is reached at U(Fe-8h) = 2.5 eV corresponding to a magnetization density of 2.54 T. Fig. 2 shows that the magnetization density saturates at around 2.58 T compared to the limiting value of 2.45 T predicted by the Slater–Pauling theory.[12] The local magnetic moments and the average magnetic moment per Fe ion as a function of U(Fe-8h) are presented in Fig. 3. The moments at Fe-8h sites are seen to increase steadily with increasing U. The moments of the Fe-4d atoms, that are located outside the Fe–N clusters, decrease and stabilize with increasing U(Fe-8h). Interestingly, the Fe-4e atoms that lie inside the

Table 2 Properties of $Fe_{16}N_2$ calculated using the GGA, GGA+U, SCAN and SCAN+U. The Hubbard U parameters used in GGA+U and SCAN+U on various Fe atoms are 1.36 eV (8h), 1.088 eV (4e) and 3.94 eV (4d). The Hubbard U parameters used in LSDA+U on various Fe atoms are 8.0 eV (8h), 1.0 eV (4e) and 1.0 eV (4d) as suggested by Ji $et~al.$[19] Magnetic moments on various Fe and N positions are given, along with the cell volume (V), the total moment per unit cell, and the magnetization density (M_s (T))

Method	Lattice parameters (Å)		V (Å^3)	Total moment (μ_B)	m: individual atom (μ_B)				M_s (T)
	a	c			Fe-8h	Fe-4e	Fe-4d	N	
GGA	5.67	6.24	200.61	38.71	2.36	2.15	2.83	−0.06	2.25
GGA+U	5.72	6.29	205.80	42.48	2.54	2.35	3.22	−0.07	2.39
SCAN	5.68	6.14	198.09	41.83	2.57	2.42	2.92	−0.05	2.45
SCAN+U	5.75	6.19	204.66	45.51	2.75	2.63	3.27	−0.05	2.58
HSE[33]	5.62	6.23	200.46	45.50	2.82	2.74	2.95	−0.05	2.64
LSDA+U	5.83	6.02	204.91	46.28	3.47	2.66	1.99	−0.06	2.63

Table 3 Properties of $Fe_{16}N_2$ calculated with the SCAN+U scheme where the Hubbard U is applied only on the Fe-8h sites

| U (eV)	Lattice parameters (Å)		V (Å^3)	Total moment (μ_B)	m: individual atom (μ_B)				M_s (T)
	a	c			Fe-8h	Fe-4e	Fe-4d	N	
0.5	5.69	6.15	199.47	42.52	2.67	2.42	2.89	−0.034	2.48
1.0	5.72	6.13	200.45	42.87	2.75	2.38	2.85	−0.036	2.49
1.5	5.73	6.13	201.11	43.24	2.84	2.34	2.82	−0.040	2.50
2.0	5.76	6.11	202.54	43.78	2.92	2.32	2.81	−0.041	2.52
2.5	5.79	6.11	204.89	44.82	3.02	2.36	2.81	−0.033	2.54
3.0	5.83	6.13	208.03	46.03	3.12	2.43	2.85	−0.021	2.57
3.5	5.85	6.14	210.16	46.67	3.19	2.44	2.86	−0.019	2.58
4.0	5.87	6.13	211.62	46.90	3.24	2.41	2.85	−0.028	2.58
4.5	5.89	6.14	213.05	47.21	3.28	2.39	2.85	−0.036	2.58
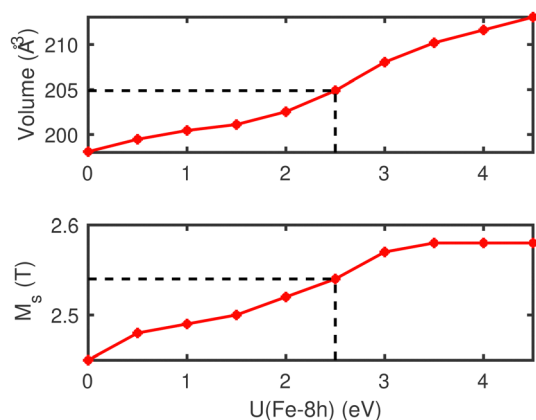
Fig. 2 Equilibrium volume and magnetization density using the SCAN+U scheme as a function of U(Fe-8h), where U is applied only to the U(Fe-8h) sites. The computed points are joined by straight lines to guide the eye. The dashed lines mark the values that reproduce the experimental moments and volume.
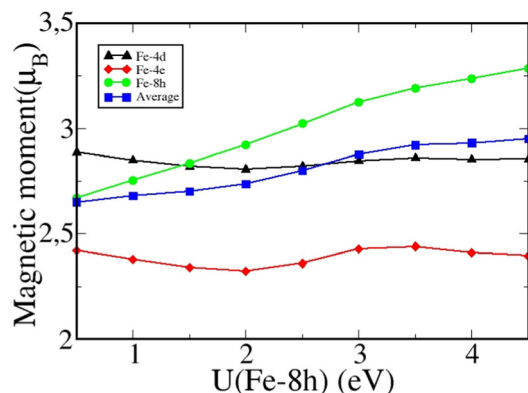

Fig. 3 Computed magnetic moments on various Fe sites and the average magnetic moment per unit cell using the SCAN+U scheme as a function of U(Fe-8h), where U is applied only to the Fe-8h sites.

Fig. 4 DOS and orbitally-projected and site-resolved partial DOSs (PDOSs) for (a) GGA, (b) SCAN and (c) SCAN+U(Fe-8h), where the Hubbard U is applied only to the Fe-8h sites. The total DOS (scaled by a factor of 0.7) is in gray, the Fe-8h e_g PDOS is in blue and the Fe-8h t_{2g} PDOS is in red shading.

Fe–N cluster also show the same trend as the Fe-4d atoms. Nevertheless, it is clear that the SCAN+U scheme, which includes self-interaction corrections within the SCAN formalism, predicts average magnetic moment of about 2.8μ_B per Fe, which is larger than the Slater–Pauling limit for itinerant ferromagnetism.

To visualize the electronic structure, we have calculated the density of states (DOS) and the partial DOSs of $Fe_{16}N_2$, see Fig. 4. The three panels of Fig. 4 present results based on GGA, SCAN and SCAN+U(Fe-8h) at $U = 2.5$ eV. The exchange splitting between the spin-up and spin-down states is seen to increase with the introduction of enhanced correlation effects: for example, the exchange splitting is larger in SCAN compared to the GGA and the addition of U(Fe-8h) further increases the exchange splitting mostly by localizing the e_g 3d states of Fe-8h. We have also carried out computations in which spin-orbit coupling effects are included for U(Fe-8h) = 2.5 eV to obtain an MCA energy of 1.3 meV per formula unit, which is consistent
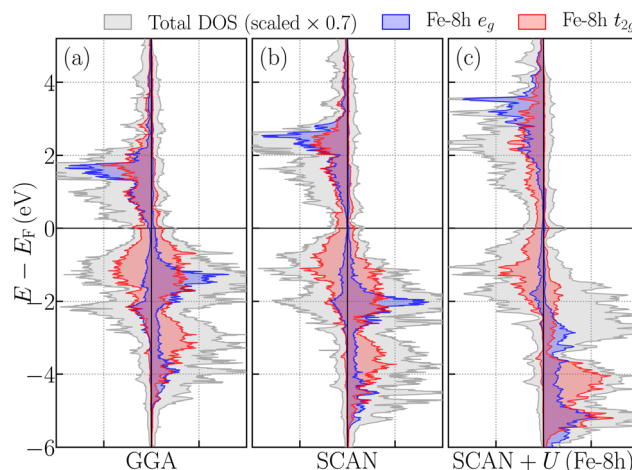
with the experimental values reported by Stoeckl et al.[22] The magnetic moments were not significantly affected by spin–orbit coupling effects.

Finally, we have performed further SCAN+U calculations in which U is applied uniformly on all Fe sites. Stoeckl et al.[22] refer to such a calculation as the baseline case, and the calculations motivated by the results of Ji et al. as the high-moment case because it gave the highest total magnetic moment within their GGA+U scheme. However, Table 4 shows that in the case of SCAN+U both the experimental volume and the giant magnetization density of 2.58 T are recovered for $U = 1.5$ eV. We have also considered a calculation applying $U = 2$ eV on Fe 8h and 4e only. The equilibrium volume in this case is 208.55 Å^3 and the magnetic moments are 2.953, 2.834 and 2.858μ_B for 8h, 4e and 4d, respectively. These values are in better agreement with the experimental values given by Hang et al.[64] while $M_s = 2.59$ T remains high. This result highlights the robustness of the SCAN+U scheme: variations in the value of U lead to different combinations of individual magnetic moments, but the experimental average magnetization and volume are obtained in all

Table 4 Properties of $Fe_{16}N_2$ calculated with the SCAN+U scheme where the U values are applied uniformly on all Fe sites

| U (eV) | Lattice parameters (Å) | | | Total moment (μ_B) | m: individual atom (μ_B) | | | | M_s (T) |
	a	c	V (Å^3)		Fe-8h	Fe-4e	Fe-4d	N	
0.5	5.70	6.15	200.33	42.89	2.64	2.53	2.95	−0.037	2.49
1.0	5.72	6.15	201.75	43.66	2.69	2.58	2.98	−0.046	2.51
1.5	5.78	6.17	205.96	45.71	2.83	2.73	3.05	−0.034	2.58
2.0	5.81	6.19	209.42	47.09	2.92	2.82	3.11	−0.041	2.62
2.5	5.85	6.21	212.38	47.90	2.97	2.89	3.16	−0.033	2.62
3.0	5.88	6.25	216.23	49.13	3.05	2.96	3.24	−0.021	2.64
3.5	5.91	6.28	220.19	50.15	3.10	3.04	3.30	−0.019	2.65

17882 | *Phys. Chem. Chem. Phys.*, 2022, **24**, 17879–17884

This journal is © the Owner Societies 2022

cases. This is important since the experimental analysis of the magnetic moment distributions remains quite challenging.[64,65]

IV. Conclusions

We have presented an in-depth study of magnetism in α''-$Fe_{16}N_2$ within the framework of the density functional theory (DFT) using a variety of schemes to treat exchange–correlation effects. The experimentally observed giant magnetization density (larger than the Slater–Pauling limit of about 2.45 T) is shown to be captured correctly by the SCAN+U scheme. Predictions of SCAN+U are robust in that magnetization densities surpassing the Slater–Pauling limit as well as the correct equilibrium volume are produced when U is applied either uniformly or unevenly across the various Fe sites. When U is applied only on the Fe-8h sites using the optimal value of 2.5 eV (yields experimental volume), Fe-3d states are localized and the largest magnetic moments on the Fe-8h sites are obtained in agreement with recent neutron diffraction experiments, etc.[18] Even when U is applied uniformly on all Fe sites using the corresponding optimal value of 1.5 eV, the total magnetic moment remains high in contrast to the GGA+U results.[22] Notably, since U promotes localization of Fe 3d electrons, problems of SCAN with Fe and other itinerant ferromagnets[56–59] do not apply to $Fe_{16}N_2$. [Location effects predicted here should be amenable to verification via magnetic Compton scattering experiments.[51,66–68]] SCAN has been successful in describing elemental Mn, which is a similar non-itinerant transition metal system.[45] Finally, we note that since correlation effects weaken directional bonding, DFT generally tends to underestimate the c/a ratio, which could be cured by including spin–orbit interactions and breaking symmetries around the iron atoms.[69]

Conflicts of interest

There are no conflicts to declare.

Acknowledgements

References

1 M. Balintova, M. Holub, N. Stevulova, J. Cigasova and M. Tesarcikova, Chem. Eng. Trans., 2014, 39, 625–630.

2 L. H. Lewis and F. Jiménez-Villacorta, Metall. Mater. Trans., 2013, 44, 2–20.

3 R. McCallum, L. Lewis, R. Skomski, M. Kramer and I. Anderson, Annu. Rev. Mater. Res., 2014, 44, 451–477.

4 L. Rissanen, M. Neubauer, K. Lieb and P. Schaaf, J. Alloys Compd., 1998, 274, 74–82.

5 T. Ogawa, Y. Ogata, R. Gallage, N. Kobayashi, N. Hayashi, Y. Kusano, S. Yamamoto, K. Kohara, M. Doi and M. Takano, et al., Appl. Phys. Express, 2013, 6, 073007.

6 T. Radchenko, O. Gatsenko, V. Lizunov and V. Tatarenko, Prog. Met. Phys., 2020, 21, 580–618.

7 K. H. Jack, Proc. R. Soc. A, 1951, 208, 216–224.

8 T. K. Kim and M. Takahashi, Appl. Phys. Lett., 1972, 20, 492–494.

9 K. H. Jack, J. Alloys Compd., 1995, 222, 160–166.

10 J.-P. Wang, N. Ji, X. Liu, Y. Xu, C. Sanchez-Hanke, Y. Wu, F. De Groot, L. F. Allard and E. Lara-Curzio, IEEE Trans. Magn., 2012, 48, 1710–1717.

11 Y. Sugita, K. Mitsuoka, M. Komuro, H. Hoshiya, Y. Kozono and M. Hanazono, J. Appl. Phys., 1991, 70, 5977–5982.

12 J. C. Slater, J. Appl. Phys., 1937, 8, 385–390.

13 J. Cadogan, Aust. J. Phys., 1997, 50, 1093–1102.

14 J. M. D. Coey, J. Appl. Phys., 1994, 76, 6632–6636.

15 M. Takahashi and H. Shoji, J. Magn. Magn. Mater., 2000, 208, 145–157.

16 J.-P. Wang, J. Magn. Magn. Mater., 2020, 497, 165962.

17 J. Liu, G. Guo, X. Zhang, F. Zhang, B. Ma and J.-P. Wang, Acta Mater., 2020, 184, 143–150.

18 X. Hang, M. Matsuda, J. T. Held, K. A. Mkhoyan and J.-P. Wang, Phys. Rev. B, 2020, 102, 104402.

19 N. Ji, X. Liu and J.-P. Wang, New J. Phys., 2010, 12, 063032.

20 S. Bhattacharjee and S.-C. Lee, Sci. Rep., 2019, 9, 1–9.

21 R. Islam and J. P. Borah, J. Appl. Phys., 2020, 128, 114902.

22 P. Stoeckl, P. Swatek and J.-P. Wang, AIP Adv., 2021, 11, 015039.

23 Y. Jiang, B. Himmetoglu, M. Cococcioni and J.-P. Wang, AIP Adv., 2016, 6, 056007.

24 Y. Shi, Y. Du and G. Chen, Scr. Mater., 2013, 68, 976–979.

25 L. Ke, K. D. Belashchenko, M. van Schilfgaarde, T. Kotani and V. P. Antropov, Phys. Rev. B: Condens. Matter Mater. Phys., 2013, 88, 024404.

26 W. Y. Lai, Q. Q. Zheng and W. Y. Hu, J. Phys. Condens. Matter, 1994, 6, L259.

27 S. Ishida, K. Kitawatase, S. Fujii and S. Asano, J. Phys. Condens. Matter, 1992, 4, 765.

28 J. Sun, A. Ruzsinszky and J. P. Perdew, Phys. Rev. Lett., 2015, 115, 036402.

29 J. P. Perdew, K. Burke and M. Ernzerhof, Phys. Rev. Lett., 1996, 77, 3865–3868.

30 R. Car, Nat. Chem., 2016, 8, 820–821.

31 J. Heyd, G. E. Scuseria and M. Ernzerhof, J. Chem. Phys., 2003, 118, 8207–8215.

32 H. Sims, W. Butler, M. Richter, K. Koepernik, E. Sasioglu, C. Friedrich and S. Blügel, Phys. Rev. B: Condens. Matter Mater. Phys., 2012, 86, 174422.

33 N. Szymanski, V. Adhikari, M. Willard, P. Sarin, D. Gall and S. Khare, J. Appl. Phys., 2019, 126, 093903.

34 J. Paier, M. Marsman and G. Kresse, J. Chem. Phys., 2007, 127, 024103.

This journal is © the Owner Societies 2022

Phys. Chem. Chem. Phys., 2022, 24, 17879–17884 | 17883

35 K. Pokharel, C. Lane, J. W. Furness, R. Zhang, J. Ning, B. Barbiellini, R. S. Markiewicz, Y. Zhang, A. Bansil and J. Sun, *npj Comput. Mater.*, 2022, **8**, 1–11.

36 G. Sai Gautam and E. A. Carter, *Phys. Rev. Mater.*, 2018, **2**, 095401.

37 G. Kresse and J. Furthmüller, *Phys. Rev. B: Condens. Matter Mater. Phys.*, 1996, **54**, 11169–11186.

38 G. Kresse and D. Joubert, *Phys. Rev. B: Condens. Matter Mater. Phys.*, 1999, **59**, 1758–1775.

39 B. Barbiellini, E. G. Moroni and T. Jarlborg, *J. Phys. Condens. Matter*, 1990, **2**, 7597.

40 S. L. Dudarev, G. A. Botton, S. Y. Savrasov, C. J. Humphreys and A. P. Sutton, *Phys. Rev. B: Condens. Matter Mater. Phys.*, 1998, **57**, 1505–1509.

41 J. P. Perdew and Y. Wang, *Phys. Rev. B: Condens. Matter Mater. Phys.*, 1992, **45**, 13244–13249.

42 M. Cococcioni and S. de Gironcoli, *Phys. Rev. B: Condens. Matter Mater. Phys.*, 2005, **71**, 035105.

43 B. Barbiellini and A. Bansil, *J. Phys. Chem. Solids*, 2005, **66**, 2192–2196.

44 A. Allerdt, H. Hafiz, B. Barbiellini, A. Bansil and A. E. Feiguin, *Appl. Sci.*, 2020, **10**, 2542.

45 A. Pulkkinen, B. Barbiellini, J. Nokelainen, V. Sokolovskiy, D. Baigutlin, O. Miroshkina, M. Zagrebin, V. Buchelnikov, C. Lane, R. S. Markiewicz, A. Bansil, J. Sun, K. Pussi and E. Lähderanta, *Phys. Rev. B*, 2020, **101**, 075115.

46 C. Lane, J. W. Furness, I. G. Buda, Y. Zhang, R. S. Markiewicz, B. Barbiellini, J. Sun and A. Bansil, *Phys. Rev. B*, 2018, **98**, 125140.

47 J. W. Furness, Y. Zhang, C. Lane, I. G. Buda, B. Barbiellini, R. S. Markiewicz, A. Bansil and J. Sun, *Commun. Phys.*, 2018, **1**, 11.

48 Y. Zhang, C. Lane, J. W. Furness, B. Barbiellini, J. P. Perdew, R. S. Markiewicz, A. Bansil and J. Sun, *Proc. Natl. Acad. Sci. U. S. A.*, 2020, **117**, 68–72.

49 J. Nokelainen, C. Lane, R. S. Markiewicz, B. Barbiellini, A. Pulkkinen, B. Singh, J. Sun, K. Pussi and A. Bansil, *Phys. Rev. B*, 2020, **101**, 214523.

50 R. Zhang, C. Lane, B. Singh, J. Nokelainen, B. Barbiellini, R. S. Markiewicz, A. Bansil and J. Sun, *Commun. Phys.*, 2021, **4**, 1–12.

51 H. Hafiz, K. Suzuki, B. Barbiellini, Y. Orikasa, S. Kaprzyk, N. Tsuji, K. Yamamoto, A. Terasaka, K. Hoshi and Y. Uchimoto, *et al.*, *Phys. Rev. B*, 2019, **100**, 205104.

52 C. Lane, Y. Zhang, J. W. Furness, R. S. Markiewicz, B. Barbiellini, J. Sun and A. Bansil, *Phys. Rev. B*, 2020, **101**, 155110.

53 J. Varignon, M. Bibes and A. Zunger, *Phys. Rev. B*, 2019, **100**, 035119.

54 H. J. Monkhorst and J. D. Pack, *Phys. Rev. B: Solid State*, 1976, **13**, 5188–5192.

55 P. E. Blöchl, O. Jepsen and O. K. Andersen, *Phys. Rev. B: Condens. Matter Mater. Phys.*, 1994, **49**, 16223–16233.

56 M. Ekholm, D. Gambino, H. J. M. Jönsson, F. Tasnádi, B. Alling and I. A. Abrikosov, *Phys. Rev. B: Condens. Matter Mater. Phys.*, 2018, **98**, 094413.

57 Y. Fu and D. J. Singh, *Phys. Rev. Lett.*, 2018, **121**, 207201.

58 Y. Fu and D. J. Singh, *Phys. Rev. B*, 2019, **100**, 045126.

59 F. Tran, G. Baudesson, J. Carrete, G. K. H. Madsen, P. Blaha, K. Schwarz and D. J. Singh, *Phys. Rev. B*, 2020, **102**, 024407.

60 D. Mejía-Rodríguez and S. B. Trickey, *Phys. Rev. B*, 2019, **100**, 041113.

61 O. Gunnarsson and B. I. Lundqvist, *Phys. Rev. B: Solid State*, 1976, **13**, 4274–4298.

62 J. M. D. Coey and P. Smith, *J. Magn. Magn. Mater.*, 1999, **200**, 405–424.

63 R. M. Metzger, X. Bao and M. Carbucicchio, *J. Appl. Phys.*, 1994, **76**, 6626–6631.

64 X. Hang, PhD thesis, University of Minnesota, 2021.

65 H. Hiraka, K. Ohoyama, Y. Ogata, T. Ogawa, R. Gallage, N. Kobayashi, M. Takahashi, B. Gillon, A. Gukasov and K. Yamada, *Phys. Rev. B: Condens. Matter Mater. Phys.*, 2014, **90**, 134427.

66 Y. Li, P. A. Montano, B. Barbiellini, P. Mijnarends, S. Kaprzyk and A. Bansil, *J. Phys. Chem. Solids*, 2007, **68**, 1556–1560.

67 H. Kobayashi, T. Nagao, M. Itou, S. Todo, B. Barbiellini, P. E. Mijnarends, A. Bansil and N. Sakai, *Phys. Rev. B: Condens. Matter Mater. Phys.*, 2009, **80**, 104423.

68 K. Suzuki, Y. Otsuka, K. Hoshi, H. Sakurai, N. Tsuji, K. Yamamoto, N. Yabuuchi, H. Hafiz, Y. Orikasa and Y. Uchimoto, *et al.*, *Condens. Matter*, 2021, **7**, 4.

69 S. Pittalis, G. Vignale and F. Eich, *Phys. Rev. B*, 2017, **96**, 035141.

17884 | *Phys. Chem. Chem. Phys.*, 2022, **24**, 17879–17884

This journal is © the Owner Societies 2022